Cochlea Modelling: Clinical Challenges and Tubular Extraction

Gavin Baker[1], Stephen O'Leary[2], Nick Barnes[1,3], and Ed Kazmierczak[1]

[1] Department of Computer Science and Software Engineering,
The University of Melbourne, 3010 Australia
gavinb@cs.mu.oz.au
[2] Department of Otolaryngology,
The University of Melbourne, 3010 Australia
[3] National ICT Australia,
Locked Bag 8001, Canberra ACT 2601 Australia

Abstract. The cochlear ear implant has become a standard clinical intervention for the treatment of profound sensorineural hearing loss. After 20 years of research into implant design, there are still many unanswered clinical questions that could benefit from new analysis and modelling techniques. This research aims to develop techniques for extracting the cochlea from medical images to support clinical outcomes. We survey the challenges posed by some of these clinical questions and the problems of cochlea modeling. We present a novel algorithm for extracting tubular objects with non-circular cross-sections from medical images, including results from generated and clinical data. We also describe a cochlea model, driven by clinical knowledge and requirements, for representation and analysis. The 3-dimensional cochlea representation described herein is the first to explicitly integrate path and cross-sectional shape, specifically directed at addressing clinical outcomes. The tubular extraction algorithm described is one of very few approaches capable of handling non-circular cross-sections. The clinical results, taken from a human CT scan, show the first extracted centreline path and orthogonal cross-sections for the human cochlea.

1 Introduction

This paper describes a collaborative project being undertaken by the Departments of Computer Science and Software Engineering, and Otolaryngology at The University of Melbourne and National ICT Australia to model and analyse the shape of the human cochlea. In the first half of the paper, we describe the problems, challenges and clinical motivations for the research. In the second half of the paper, we present a novel algorithm for extracting tubular objects with non-circular cross-sections (such as the cochlea) from medical images. We present results from generated test data, and clinical results from human CT scans.

G.I. Webb and Xinghuo Yu (Eds.): AI 2004, LNAI 3339, pp. 74–85, 2004.

2 Clinical Background

Across the world, millions of people suffer from profound sensorineural hearing loss. This form of deafness affects many people; one in 1000 babies are born deaf with congenital hearing defects, while adults can develop profound hearing loss with age. Around 40% of people over the age of 75 and over 3 million children suffer from hearing loss. Until recent years, this type of hearing loss was incurable. Nerve-impaired deafness is not treatable with standard acoustic hearing aids, which only amplify the sound. It is characterised by damage to the nerve or hair cells in the inner ear, and has a variety of causes.

In normal human hearing, sound waves enter the outer ear via the *external auditory meatus* (ear canal) and strike the *tympanic membrane* (ear drum). This resonates the connected *auditory ossicles* (middle ear bones) which convert the sound waves into mechanical vibration that in turn resonates via the round window along the *scala* (internal channel) of the *cochlea* (shell-like hearing organ). The vibrations displace the *basilar membrane*, which runs the length of the cochlea. Hair cells attached to the membrane are displaced by the vibration and generate an electrochemical stimulus causing neurons in the local region to fire. The neuronal stimulus is transmitted via the *auditory nerve* to the cortex of the brain for processing. The sound frequency is a function of the distance along the cochlea, thus spatially encoding sound.

The cochlea is the organ of hearing, a tiny (2cm^3) shell-like spiral structure in the inner ear, embedded in the temporal bone of the skull. A normal cochlea revolves through $2\frac{1}{2}$ turns, from the *basal turn* (lower turn) up to the *helicotrema* (top of spiral). Three channels run the length of the cochlea: the *scala tympani*, *scala media* and *scala vestibuli*. The cochlear implant (described below) is inserted into the scala tympani. The path of the cochlea resembles a helical spiral, while the cross-sectional shape resembles a cardioid (rounded "B" shape). The *basilar membrane* resonates at different frequencies along its length; the distance along corresponds to the frequency perceived. The degree of neuronal stimulation determines the amplitude (volume) sensed.

The cochlear implant, also known as the bionic ear, was developed by Professor Graeme Clark at The University of Melbourne and later at The Bionic Ear Institute. The implant restores hearing to patients with sensorineural damage, and has become a standard clinical intervention for profound deafness. There have been over 50,000 recipients of the cochlear implant in 120 countries worldwide, since the first clinical trials in 1985 [2].

The cochlear ear implant consists of: an external microphone that picks up sound; a signal processing unit that converts the sound into electrical signals; and an electrode array that stimulates the nerve fibres inside the cochlea. This completely bypasses the outer and middle ear, and relies only on residual hearing in the form of viable neurons inside the cochlea. The signal processing unit performs spectrum analysis on the incoming sound, and determines the frequency and amplitude of the speech. The array consists of a series of electrodes that directly stimulate the auditory nerve with electrical current, thus recreating

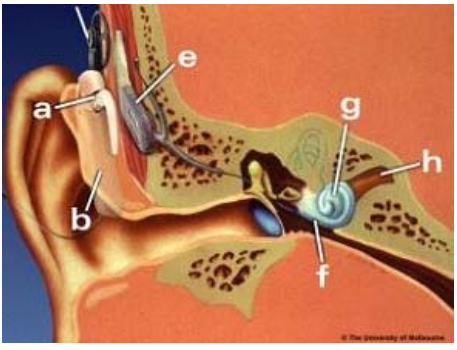

Fig. 1. Left: The middle and inner ear: a) external cochlea device, b) signal processor, f) basal turn, g) cochlea, h) auditory nerve

the sensation of hearing. The distance along the array encodes frequency, while current determines amplitude [3].

There are many clinical problems and questions that could benefit from new techniques for the analysis of the shape of the cochlea and implant, some of which are listed in Figure 2. In order to answer these questions, it is clear that

1. *Does the patient suffer from Mondini's syndrome [1]?*

A normal cochlea revolves about $2\frac{1}{2}$ turns, whereas Mondini's syndrome is characterised by incomplete formation of turns. This needs a model of the cochlea path to determine number of turns of cochlea canal.

2. *Does the patient present surgical risks?*

Pathologies such as ossification of the basal turn can complicate surgery. A model of cross-sectional shape could identify such an abnormality, given a statistical prior model of normal shape.

3. *Where are the electrodes with respect to the modiolus?*

Calibration and tuning of the speech processor are affected by the distance to the modiolus and the position of each electrode. This requires a cochlea model and implant model to determine distances and path.

4. *How far has the electrode array been inserted?*

Post-operative tuning of the signal processor depends on this information, to determine frequency correspondences with the electrodes. Requires a model of the cochlea and implant.

5. *Has the implant pierced the basilar membrane?*

If this occurs during implant insertion, it may impair vestibular function or damage residual neurons. This information may also be used to improve electrode design, and have impact on surgical technique evaluation. Requires detailed cochlea model and implant model.

Fig. 2. Clinical questions, surgical outcomes and cochlea modelling requirements

we need a shape model of the cochlea that captures the path of the *otic capsule*, the cross-sectional shape (along with the position of the basilar membrane), and a model of the path of the implant with respect to the cochlea model.

Abnormalities in the shape of the cochlea may be associated with hearing impairment and deafness. Shape analysis of the cochlea also has implications for cochlear implant surgery in several areas: diagnosis, such as identifying Mondini's syndrome [1] and ossification of the basal turn; surgery planning, since vital structures may be found in unpredictable locations; and clinical management, as abnormal shape increases the risk of meningitis.

A variety of non-invasive imaging techniques are available to clinicians for diagnosis and surgery planning. Conventional 2D x-rays, or *radiographs*, have been in use for many years, and are still widely used. *Computed Tomography* (CT) is a form of 3-dimensional x-ray, which is particularly suited to imaging bone structures. *Magnetic Resonance Imaging* (MRI), also a 3-dimensional modality, images the subject in a magnetic field, and is best at discriminating different types of tissue. Since the implant is metallic, MRI cannot be used post-operatively, due to the risk of internal damage. X-rays and CT scans are currently the only practical means of post-operative evaluation *in vivo* for cochlear implant patients.

There are clearly many clinical motivations for imaging the cochlea. However, there are many significant challenges that remain before these questions can be answered. As the cochlea is only 2cm^3 (about the size of a marble), with current imaging resolutions, *in vivo* scans will resolve approximately 60x60x45 voxels at a 0.1mm anisotropic scale. The *scala tympani*, the part of the cochlea into which the electrode is inserted, is approximately 1mm in diameter. The electrode itself consists of 24×0.01mm wires with electrodes of 0.5mm in diameter.

Traditional 2D radiographs are currently used in clinical practice to post-operatively evaluate the position of the electrode. The individual wires and electrodes on the implant are visible, and the resolution is very good. However, it can be difficult to acquire an x-ray that is properly aligned with the basal turn. More significantly, since the radiograph is a planar projection, 3D information is lost. Current clinical practice relies on the surgeon's experience to make qualitative evaluations from this data. A CT scan can deliver a full 3D reconstruction of the cochlea and electrode array post-operatively. However, the metallic construction of the electrode (platinum) introduces significant blooming artifacts into the surrounding image, and distorts for more than 1mm. Individual electrodes are not detectable in CT [4]; only the path of the implant and wires. Since this distortion extends beyond the size of the cochlea affecting local structures, post-operative evaluation of the implant path is not ordinarily feasible. Clearly, neither CR nor CT is sufficient alone for these evaluations.

Surprisingly little attention has been paid to modelling the three-dimensional shape of the hearing organ itself, the cochlea. It is generally accepted that the cochlea resembles an Archemidean spiral [5, 6] or shell. The only models published have described the path, thus no model integrating path and cross-section exists.

Cohen's 2D Electrode Model. Cohen *et al.* present a 2-dimensional spiral template to model the path of the inserted electrode array [7], providing a model for frequency estimation and implant tuning. This can be seen as an approximation of the path of the *otic capsule* (defined by the walls of the bone structure containing the cochlea), however it is known that the implant does not always track the walls. Since the implant is inserted into the scala tympani, the electrode will not necessarily follow the precise centreline of the otic capsule itself. Thus this model is only an approximation to the cochlea tubular path.

Cohen's 2D spiral model is a piecewise logarithmic spiral based on a polar co-ordinate system (the second equation takes into account the curvature of the basal turn):

$$\begin{aligned} R &= ac^{-b\theta} && \theta \geq 100^\circ \\ R &= c(1 - d\log(\theta - \theta_0)) && \theta < 100^\circ \end{aligned} \tag{1}$$

for some constants a, b, c, d. The origin is centred at the modiolus.

Yoo's 3D Spiral Model. Cohen's 2D electrode path model was extended into 3D by Yoo *et al.* [5, 8] in order to model the centreline path of the cochlea itself. This involved adding a Z-axis component to the existing polar coordinate system. First a linear function $z = e(\theta - \theta_1)$ was described [5], then an exponential function $h = ce^{d\theta}$ [8], where z and h both represent the height of the spiral curve, for some constants c, d, e and angle θ.

This model for the cochlea centreline is based on the electrode model, and assumes that the paths are coincident. It was evaluated on a single patient and validated against histological data, which is typically imprecise. The centreline is taken as the centroid of cross-section, which is extracted using Wang's unwrapping technique [9]. Ultimately this model is only an approximation to the path of the cochlea centreline; it does not address the shape of the cross-section of the cochlea along its path.

Ketten's Archimedean Spiral Model. Ketten *et al.* present an Archemidean spiral model, which is used to estimate cochlea length along the midcanal spiral path [6]. This model is aimed at predicting insertion depth and cochlea length, and thus does not directly address the 3D space-curve path that we seek. Yoo points out that this model does not take into account the basal turn [8], and thus is less faithful to cochlea morphometry than the models described above.

Models Summary. The most advanced model thus far is the 3D path model of Yoo *et al.*. It been derived from a single CT scan, is based on the assumption that the electrode path and centreline are equivalent, and does not address cross-section. These existing models are inadequate to respond to the clinical questions before us. This research aims to address this gap by producing a model that integrates both path and cross-sectional shape, developing an extraction algorithm capable of generating such a model, and one that will integrate with a model of the electrode.

3 Tubular Object Extraction

The cochlea is often described as an Archemidean spiral shell [5], which can be approximated by a logarithmic curve. However the cross-sectional shape of the cochlea is not elliptical; it resembles a cardioid (a rounded "B"). Both the shape and size of the cochlea vary along its length, posing some unique challenges for extraction and modeling. Most existing tubular extraction techniques are concerned with the vasculature, where a circular or elliptical cross-section is typically assumed. Since we cannot make this assumption, a new approach is required that explicitly treats complex cross-sectional shape. Our goal is therefore to develop techniques for extracting 3-dimensional tubular objects with non-circular cross-sections, and recover clinically relevant parameters that support medical outcomes.

The remainder of this paper is structured as follows: first we discuss related research in the area of tubular object extraction, and why these are unsuitable for our purposes. Then we describe the design of our algorithm, including parameter selection. We then present the results of processing synthetic data (a gold standard) based on Yoo's 3D model, and real CT dataset of a human cochlea.

A number of approaches exist for tubular object segmentation and extraction, however the majority of research has focused on segmenting vascular networks [10–14]. Since blood vessels are thin, long, have circular or elliptical cross-sections and form complex branching networks, most tubular research has focused on anatomy with these attributes. Consequently, larger tubular objects with non-trivial cross-sections such as the cochlea have received much less attention.

The intrinsic shape characteristics of a tube can be described by two related components: the *centerline path* and the *cross-sectional shape* along the path. Binford [15] first proposed the Generalised Cylinder (GC), a spatial curve defining the centerline path of the object, and a cross-section (typically circular or elliptical) that can vary as a function of the distance along the path. The Right Generalised Cylinder (RGC) [16] constrains the cross-section to be orthogonal to the tangent of the path. With some exceptions (eg. [13]), the majority of recent approaches to tubular models employ variations on the RGC. In the case of the cochlea, the centerline path is clinically significant (see Figure 2). Consequently, a tubular representation suitable for shape analysis would be highly desirable.

In scale space terms, the *gross-scale* shape of a tube is characterised by the path of its centerline (the tubular axis), and is typically modelled as a B-spline [11]. To extract the centreline of a tube, Principal Components Analysis (PCA) can be applied to a local image region directly to track the maximal eigenvector [9] and follow the principal axis. More common is to apply PCA to the local Hessian matrix, and track along the maximal eigenvectors [10, 11, 14].

Aylward *et al.* [10] use multi-scale intensity ridge traversal, driven by the eigenvalues of the local Hessian, to extract the centerline of blood vessels. This approach requires a near-circular cross-section, limiting its applicability to complex cross-sectional modeling. While Krissian [14] simply employs the local Hessian for orientation, Frangi [11] also employs a local discriminant function that identifies tubular structures locally to improve and guide tracking.

The Hessian is a 2^{nd}-order directional derivative, which makes it more susceptible to noise than a 1^{st}-order gradient operator (employed in our approach). Multi-scale blurring is typically used in conjunction with the local Hessian to mitigate noise. This also ensures the requisite Gaussian intensity profile to create the intensity ridge at the centre of the tube. However, this requires the cross-section to be nearly circular [10], thus limiting its generality. Bifurcations can also cause problems when using the local Hessian, due to filtered signal loss around the joint [11].

Yim *et al.* [13] employ a deformable curve (*snake*) in a novel tubular coordinate system, that deforms according to image and smoothing forces to model the wall as a mesh. It is assumed that the centerline has been manually specified as a sequence of points along the centre axis of the vessel, although Bitter [17] demonstrates how this can be error-prone.

Lorigo describes an approach based on Level Sets called CURVES [12], that uses an evolving curve driven by image intensity gradient to extract vasculature. However the result is still a segmentation, and thus further analysis would be required to produce a tubular model suitable for shape analysis.

The *fine-scale* detail of a tube is defined by the local shape of the orthogonal cross-section, which can vary along the length of the tube. This is difficult to extract and model explicitly. Most approaches either do not address cross-sectional shape [18], or assume a circular or elliptical [10] cross-section. These assumptions may generally be valid for vasculature, however in [11] Frangi points out that "*ex vivo* measurements have shown that this assumption is rather simplistic". Frangi describes a spline-based tubular model capable of representing non-circular cross-sections, and demonstrates the approach to model vessel stenosis.

3.1 Tubular Extraction Algorithm

The Tubular Extraction algorithm uses the *Principal Flow Filter* [19] to incrementally extract a tubular object by tracking along its path and taking cross-sectional slices. Since our approach is driven by the image gradient at the tube walls, there is no constraint imposed on the cross-sectional shape. In this paper, we do assume that the cross-sectional area does not vary significantly along the length, which is valid for the cochlea.

The Principal Flow Filter calculates the local orientation of flow along a tube. Given an input volume $I : \mathbb{R}^3 \mapsto \mathbb{R}$ containing a non-branching tubular object, we specify a point $\mathbf{p} = (x, y, z)$ inside the tube, and a vector $\boldsymbol{v}$ oriented approximately along the tube. We assume that the contrast along the tubular walls is strong (see Figure 3(a)). Thus the gradient intensity vectors along the walls will tend to be oriented approximately co-planar with the orthogonal cross-sectional plane. It follows that the cross-product of any two of these wall gradient vectors should produce a vector approximately oriented along the tubular axis. With a sufficiently robust analysis, a local region can be processed in this way to calculate a mean orientation from all the cross-products, yielding the principal flow vector $\boldsymbol{v}_f$.

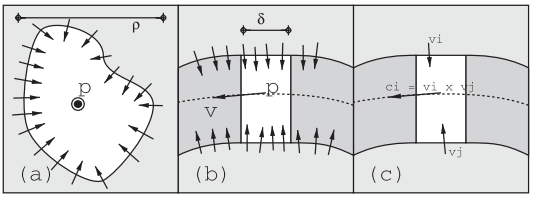

Fig. 3. (a) Cross-section of a tube, showing: centroid $\mathbf{p}$, maximal diameter ρ, and gradient vectors around wall; (b) Side view of tube, showing: point $\mathbf{p}$, flow vector $\boldsymbol{v}_f$, longitudinal dimension δ and gradient vectors along the wall; (c) pairs of gradient vectors along the wall contribute to flow vector

Parameters are supplied for the expected maximum diameter of the tube ρ and the desired section depth δ (inversely proportional to the curvature). This specifies a Volume of Interest $\mathcal{V}$, centred at $\mathbf{p}$, oriented such that $\boldsymbol{v}$ defines the new Z-axis, with size $\rho \times \rho \times \delta$. We size $\mathcal{V}$ such that it completely encloses a short and relatively uniform section of the tube; that is, the width and height ρ is slightly larger than the diameter of the tube, and the depth δ is small enough to minimise local curvature. Over the resampled VOI $I_{\mathcal{V}}$ we calculate the first-derivative image gradient:

$$\boldsymbol{G} = \nabla I_{\mathcal{V}} \tag{2}$$

Thus $\boldsymbol{G}$ will yield strong gradient vectors normal to the walls. We randomly sample N vectors $\boldsymbol{a}$ from this vector field:

$$\boldsymbol{M} = \{\boldsymbol{a}_i : \boldsymbol{a}_i = S(\boldsymbol{G}), i \in [0, N], \|\boldsymbol{a}_i\| > \epsilon\} \tag{3}$$

where S is a pseudo-random sampling function, and ϵ is the minimum gradient magnitude threshold. We then take the vector cross-product of all pairs from $\boldsymbol{M}$:

$$\mathcal{C} = \{c_i : c_i = v_m \times v_n, \forall v_m, v_n \in \boldsymbol{M}, m \neq n\} \tag{4}$$

We map the vectors from $\mathcal{C}$ into $(\phi, \psi) \in \mathbb{R}^2$, where ϕ is the angle of $\boldsymbol{c}_i$ in the XZ plane and ψ is the angle of in the YZ plane (see Figure 4(c)). This produces a cluster around the mean local orientation. To eliminate outliers and mitigate against sampling noise, we employ a robust random sampling approach based on the RANSAC algorithm [20]. A series of potential models is taken from the data set, and compared with all data points in the set using a Euclidean distance metric $d(\boldsymbol{a}, \boldsymbol{b})$. The support for a model is increased by a data point falling within a given threshold of the model. After a sufficient number of iterations, the model with the greatest support is chosen. The new mean orientation is calculated from all points in this support set, which is transformed back into a vector in the original frame, and becomes the local flow vector $\boldsymbol{v}_f$ for that region oriented along the tube.

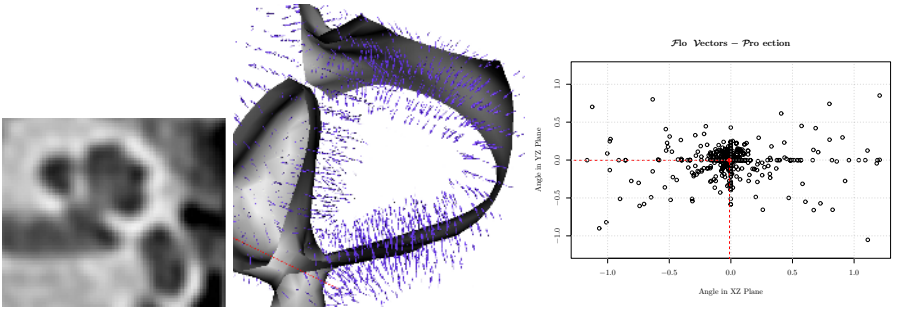

(a) (b) (c)

Fig. 4. (a) typical mid-saggital slice of human cochlea, showing upper and basal turns, and auditory nerve; (b) A VOI from the CT cochlea, showing wall with gradient vectors; (c) Flow vectors projected into a Euclidean space, with a cluster clearly showing consensus on orientation

The *Tubular Extraction* algorithm consists of the following steps:

1. Initialise with $\mathbf{p} = \mathbf{p}_0$ and $\boldsymbol{v} = \boldsymbol{v}_0$, and select ρ, δ
2. Resample the Volume Of Interest (VOI) centred at $\mathbf{p}$ oriented by $\boldsymbol{v}$, with dimensions $\rho \times \rho \times \delta$
3. Calculate the local flow direction $\boldsymbol{v}_f$ using the Principal Flow Filter
4. Extract the cross-sectional plane $\mathcal{P}$ given normal $\boldsymbol{v}_f$ centred about $\mathbf{p}$
5. Calculate the new centre $\mathbf{p}_c$ from centroid of $\mathcal{P}$
6. Calculate the new centre point with $\mathbf{p} = \mathbf{p}_c + \delta \boldsymbol{v}_f$
7. Repeat from step 2

3.2 Results

First the algorithm was evaluated against generated data, in order to have ground-truth for testing and validation. Yoo's 3D model of the cochlea [5] was used to generate a realistic test model (Figure 5i,ii). Two test volumes were rendered with different cross-sections: a circular shape with diameter 10mm, and a clover-leaf shape with diameter 12mm (resolution 1mm/voxel). The tracking results are shown in Figure 5 (iii,iv). The algorithm demonstrated excellent tracking in both cases, successfully extracting the entire length of the tubes automatically.

The algorithm has also been applied to a CT scan of a real human cochlea. The input data and tracking results are shown in Figure 5. The algorithm successfully tracked through the basal and mid-modiolar sections of the cochlea, for approximately $1\frac{1}{4}$ turns. The characteristic curve shape is clearly visible in the XZ plot of Figure 6(iv). At two points, anatomy adjoins the cochlea, creating a bifurcation that necessitated a manual restart. The tracking is not precisely on the centreline, mainly due to the low resolution available (limited by clinical considerations and x-ray dosage).

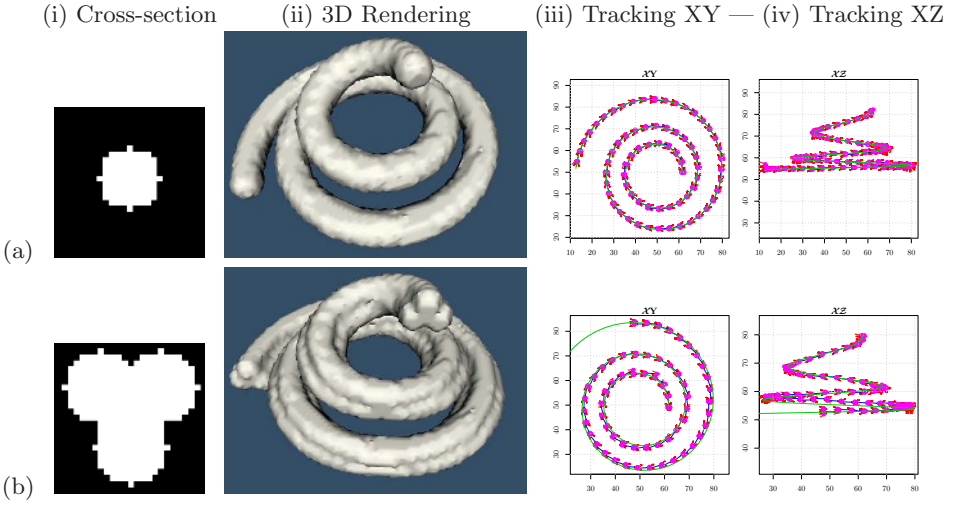

Fig. 5. Generated Data: Input data (i,ii) and tracking results (iii,iv) for (a) circular and (b) clover cross-section

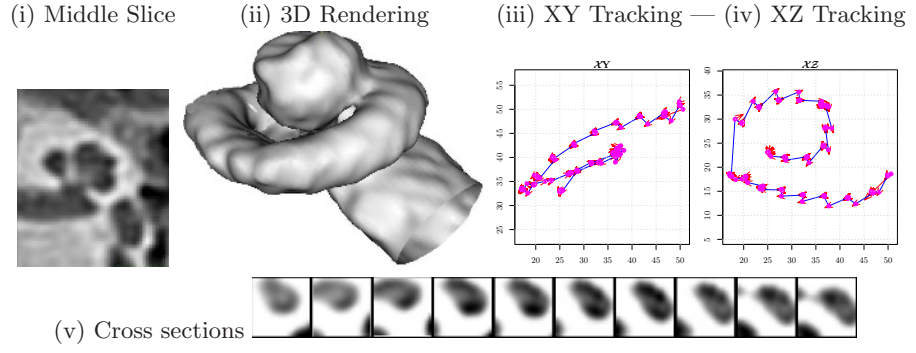

Fig. 6. Clinical Results: the input CT scan data showing a mid slice (i) and 3D view (ii), with tracking results (iii,iv) and the first 10 cross-sections (v). Note: the path in (iii) is not orthogonal to viewing plane

4 Conclusion

We have presented a survey of the clinical challenges of cochlea modelling. We have presented a novel tubular extraction algorithm that captures the path of tubular objects and their cross-sections. The algorithm explicitly handles non-circular cross-sections, which is relevant to numerous areas of anatomy. The output of the algorithm is model-centric, which has direct advantages for shape analysis, as the model directly captures clinically relevant parameters. The results demonstrated very accurate extraction of difficult generated test data. Sig-

nificantly, the algorithm has been applied to CT and produced the first successful of the centreline and cross-sections of the human cochlea for $1\frac{1}{4}$ turns. This data will be validated, extended to analyse a small population, and form the basis of the first general cochlea shape model derived from clinical data. The challenge of bifurcations will need to be addressed to apply this technique to other anatomy.

Our thanks to the Royal Victorian Eye and Ear Hospital for supplying the CT scan data used in this study, to the reviewers for their helpful comments, and to the developers of the Insight Toolkit [21] imaging library, which was used to develop the analysis software for this project.

References

1. Mondini, C.: Anatomia surdi nati sectio: Bononiensi scientiarum et artium instituto atque academia commentarii. Bononiae **7** (1791) 419–431
2. The Bionic Ear Institute, Melbourne, Australia: About the bionic ear. `http://www.bionicear.org/bei/AboutHistory.html` (2004)
3. Loizou, P.: Introduction to cochlear implants. IEEE Engineering in Medicine and Biology (1999) 32–42
4. Whiting, B., Bae, K., Skinner, M.: Cochlear implants: Three-dimensional localisation by means of coregistration of CT and conventional radiographs. Radiology **221** (2001) 543–549
5. Yoo, S., Rubinstein, J., Vannier, M.: Three-dimensional geometric modeling of the cochlea using helico-spiral approximation. IEEE Transactions on Biomedical Engineering **47** (2000) 1392–1402
6. Ketten, D., Skinner, M., Wang, G., Vannier, M., Gates, G., Neely, G.: In vivo measures of cochlear length and insertion depth of nucleus cochlea implant electrode arrays. Ann. Otol., Rhinol. Laryngol. **107** (1989) 515–522
7. Cohen, L., Xu, J., Xu, S., Clark, G.: Improved and simplified methods for specifying positions of the electrode bands of a cochlear implant array. American Journal of Otology (1996)
8. Yoo, S., Wang, G., Rubenstein, J., Skinner, M., Vannier, M.: Three-dimensional modeling and visualisation of the cochlea on the internet. IEEE Transactions on Information Technology in Biomedicine **4** (2000) 144–151
9. Wang, G., Vannier, M., Skinner, M., Kalender, W., Polacin, A., Ketten, D.: Unwrapping cochlear implants by spiral CT. IEEE Transactions on Biomedical Engineering **43** (1996) 891–900
10. Aylward, S., Bullitt, E.: Initialization, noise, singularities, and scale in height ridge traversal for tubular object centerline extraction. IEEE Transactions on Medical Imaging **21** (2002) 61–75
11. Frangi, A., Niessen, W., Hoogeveen, R., van Walsum, T., Viergever, M.: Model-based quantitation of 3-D magnetic resonance angiographic images. IEEE Transactions on Medical Imaging **18** (1999) 946–956
12. Lorigo, L.M., Faugeras, O.D., Grimson, W.E.L., Keriven, R., Kikinis, R., Nabavi, A., Westin, C.F.: CURVES: Curve evolution for vessel segmentation. Medical Image Analysis **5** (2001) 195–206
13. Yim, P., Cebral, J., Mullick, R., Marcos, H., Choyke, P.: Vessel surface reconstruction with a tubular deformable model. IEEE Transactions on Medical Imaging **20** (2001) 1411–1421

14. Krissian, K., Vaillant, G.M.R., Trousset, Y., Ayache, N.: Model-based multiscale detection of 3D vessels. In: Computer Vision and Pattern Recognition, IEEE (1998) 722–727
15. Binford, T.: Visual perception by computer. In: IEEE Conference on Systems Science and Cybernetics. (1971)
16. Zerroug, M., Nevatia, R.: Three-dimensional descriptions based on the analysis of the invariant and quasi-invariant properties of some curved-axis generalized cylinders. IEEE Transactions on Pattern Analysis and Machine Intelligence **18** (1996) 237–253
17. Bitter, I., Sato, M., Bender, M., McDonnell, K.T., Kaufman, A., Wan, M.: CEASAR: a smooth, accurate and robust centerline extraction algorithm. In: Proceedings of the conference on Visualization '00, IEEE Computer Society Press (2000) 45–52
18. Flasque, N., Desvignes, M., Constans, J.M., Revenu, M.: Acquisition, segmentation and tracking of the cerebral vascular tree on 3D magnetic resonance angiography images. Medical Image Analysis **5** (2001) 173–183
19. Baker, G., Barnes, N.: Principal flow for tubular objects with non-circular cross-sections. In: Proceedings of the International Conference on Pattern Recognition, Cambridge, England (2004)
20. Fischler, M.A., Bolles, R.C.: Random sample consensus: a paradigm for model fitting with applications to image analysis and automated cartography. Communications of the ACM **24** (1981) 381–395
21. Ibáñez, L., Schroeder, W., Ng, L., Cates, J.: 1. In: The ITK Software Guide. Kitware Inc (2003)